frontiers | Frontiers in Physics

TYPE Original Research
PUBLISHED 04 December 2024
DOI 10.3389/fphy.2024.1498648

OPEN ACCESS

EDITED BY
Francisco Vega Reyes,
University of Extremadura, Spain

REVIEWED BY
Shuihua Zheng,
Zhejiang University of Technology, China
Michael Booty,
New Jersey Institute of Technology, United States
Wei Li,
Jiangsu University, China

*CORRESPONDENCE
Guangtai Shi,
15884985712@163.com

RECEIVED 19 September 2024
ACCEPTED 18 November 2024
PUBLISHED 04 December 2024

CITATION
Guo X, Shi G, Chai H, Lv W and Fu J (2024) Influence of speed on the internal flow characteristics of a multiphase pump based on a coupled CFD-PBM model.
Front. Phys. 12:1498648.
doi: 10.3389/fphy.2024.1498648

Influence of speed on the internal flow characteristics of a multiphase pump based on a coupled CFD-PBM model

Xin Guo, Guangtai Shi*, Hongqiang Chai, Wenjuan Lv and Jie Fu

Key Laboratory of Fluid and Power Machinery (Xihua University), Ministry of Education, Chengdu, China

Under the influence of the characteristic behavior of the bubbles, the flow pattern in the multiphase pump suffers a serious deterioration and the pressurization performance is significantly reduced. In order to be more close to the engineering practice, the CFD-PBM (Computational Fluid Dynamics-Population Balance Model) coupling model is established and verified on the basis of considering the bubble coalescence and breakup behavior, revealing the bubble distribution characteristics in the pressurization unit, and studying the influence of speed on the internal flow characteristics of the multiphase pump. The results show that the volume fraction of large bubbles in the pressurization unit of the multiphase pump decreases significantly with increasing speed, and the bubble coalescence zone shrinks parallel to the blade profile along the flow direction. The volume fraction of small bubbles increases sharply with speed, and the bubble breakup zone covers almost the entire fluid domain at high speed conditions. The speed has a significantly greater influence on the distribution of the gas phase and the vortex structure in the diffuser domain than in the impeller domain. In the diffuser domain, a pair of mutually separate vortices are formed, and a large number of gas phases are sucked near the vortex center. With the increase of speed, the velocity slip in impeller domain is weakened, but in diffuser domain is intensified. The results of the study can accurately predict the performance variation of the multiphase pump and are important for their optimal design and engineering application.

KEYWORDS

multiphase pump, CFD-PBM coupling model, bubble distribution, speed, internal flow characteristic

1 Introduction

Energy serves as a fundamental basis and support for national prosperity and sustainable economic development, and it is being actively and efficiently harnessed in response to the continuous increase in human energy demand. As terrestrial resources become increasingly depleted, research indicates that marine resources possess significant potential; consequently, the exploration and transportation of offshore oil and gas are rapidly emerging as key areas of focus in scientific inquiry. In the transportation of complex mixtures comprising natural gas and impurities such as

sand and gravel, multiphase pumps are extensively utilized in offshore oil fields due to their compact design, versatility under varying operating conditions, and resistance to wear [1]. In practical engineering applications, the intricate bubble flow conditions at the pump impeller inlet exhibit a range of dynamic characteristics. The multiphase flow is inevitably accompanied by phenomena such as gas-liquid separation, bubble coalescence, and breakup. When the gas volume fraction (GVF) is high, the air bubbles within the vane pump flow channel frequently collide with one another. This interaction, particularly involving larger bubbles, can lead to blockages in the flow channel or even result in pump air lock phenomena, causing the pump to operate idly [2–4].

This paper focuses on the axial multiphase pump as the subject of study due to its intricate structure and the variability of flow patterns within its passage, which complicates the exploration of flow mechanisms in a multiphase environment. Recent advancements in optics, laser technology, and computer science have led to significant refinements in flow field testing techniques by researchers both domestically and internationally, enabling the precise capture of complex flow patterns. [5, 6] were the first to employ visualization techniques to examine the gas-liquid flow state in a centrifugal pump. Their findings indicated that a small quantity of bubbles present at low gas volume fractions (GVF) exacerbated the non-uniformity of flow velocity, with the mainstream shifting towards the suction side of the blade. Furthermore, as GVF increased, a significant number of bubbles emerged within the pump and gradually evolved into elongated gas pockets accumulating at the impeller inlet. [7] found in his study that the gas pockets formed at very high GVF would lead to plug flow in the passage and defined specific values for the cross-sectional GVF at which bubble flow occurs in the impeller of a centrifugal pump, arguing that the path of motion of the bubbles is shifted along the flow direction from the suction side of the blade to the pressure side. [8] classified the gas-liquid two-phase flow pattern inside a centrifugal pump into four flow patterns: isolated bubble flow, bubble flow, gas pocket flow and gas-liquid separation flow by visualization techniques and found that the pump performance dropped sharply when the inlet GVF was higher than 6.2%. In order to enhance the uniformity of gas-liquid mixing and thus improve the flow pattern, [9] revealed the variation of gas-liquid two-phase flow pattern and bubble diameter at the inlet of the multiphase pump under different working conditions after setting up a homogenizer at the front of the multiphase pump. The results indicate that the incorporation of a homogenizer leads to a more uniform distribution of bubbles within the flow passage and significantly reduces bubble aggregation phenomena, thereby enhancing the delivery performance of the multiphase pump. [10] used high speed photography to obtain the trajectory of bubbles in a centrifugal pump and investigated the effect of parameters such as bubble diameter and liquid phase flow rate on the trajectory of the bubbles in combination with numerical calculations. The results indicate that the movement of bubbles within the impeller is hindered as both the diameter and rotational speed of the impeller increase; conversely, an enhancement in liquid flow rate facilitates bubble movement.

With the rapid development of computer resources and numerical calculation methods, CFD has been widely used in complex engineering and has become an important tool for studying the mechanism of multiphase flow in fluid machinery [11]. [12, 13] used computational fluid dynamics to study the vortex flow patterns and energy loss of a mixed-flow pump and systematically proposed an energy characteristic optimization method based on response surface models. [14, 15] first predicted the gas-liquid two-phase flow in a centrifugal impeller at low GVF conditions based on the bubble flow model, and then proposed a new bubble flow model at high GVF conditions assuming that the bubbles would coalescence with each other and attach to the impeller surface to form fixed cavities. [16, 17] used a two-fluid model to give a three-dimensional numerical calculation of an electric submersible pump and obtained the distribution characteristics of each phase of the medium inside the impeller, and found that the bubble diameter was the key to the simulation accuracy, and the accumulation of bubbles inside the impeller was the main reason for the deterioration of the pump performance. [18] explored the forces acting on bubbles in centrifugal pumps without considering the compressibility of the medium and found that the lift forces on the bubbles themselves and the interaction between the bubble population could not be ignored when the gas content was above 3%. Tremante *et al.* [19] proposed a modified multiphase flow model that is more applicable to low GVF, and conducted a numerical simulation study of a spiral axial flow pump, revealing the influence of the gas phase fraction on the force between the gas and liquid phases, and the existence of bubbles and stratified flow within the impeller was effectively confirmed. [20] and [21] studied the effect of bubble size on the flow of an electric submersible pump under two-phase flow conditions with numerical simulations as the main focus, supplemented by experimental validation, which provided assistance in the validation and improvement of new bubble analysis models.

As can be seen, the performance of rotating machinery in a gas-liquid environment is inextricably linked to the flow pattern in the flow passage, the dynamics of the bubbles, etc. The movement of the bubbles within the impeller and the morphological changes such as coalescence and breakup will directly lead to changes in the flow pattern within the pump, thus making the performance of the pump affected [22, 23]. To more accurately capture the flow field information of rotating machinery within a gas-liquid mixed transport environment and to comprehend the temporal variations of key parameters for each phase in the flow passage, a CFD-PBM model has been used that integrates the predictive capabilities of computational fluid dynamics (CFD) with the advantages of population balance modeling (PBM) for calculating discrete phase particle size distribution and variation, thereby aligning more closely with actual application systems. Initially, the model was mainly applied to equipment such as bubble towers and stirred kettles with relatively simple structures. [24] first established equilibrium equations for the particle size variation of solid particles in chemical processes, which clearly described the bubble size distribution and the bubble coalescence and breakup phenomena in the reactor. Subsequently, [25, 26] from Tsinghua University proposed a CFD-PBM model in a gas-liquid (slurry) reactors to quantify the bubble size distribution in different bubbling zones and modified the model after considering the forces between the gas and liquid phases. On this basis, [27] revealed the effects of viscosity and distributor on gas phase parameters such as bubble volume fraction, bubble size and gas-liquid phase velocity within the bubbling bed by developing and validating a new breakup model. After the maturity and widespread use of PBM within gas-liquid two-phase flows, scholars have

extended them to rotating machines with their complex structures. [28] completed the first numerical simulation of a coupled CFD-PBM model within a split blade pump and compared it with the flow field under fixed size bubble conditions to verify the validity of the PBM model when simulating a centrifugal pump. [29] used CFD-PBM to numerically simulate the full flow passage of a gas-liquid two-phase centrifugal pump, and found that as the inlet GVF increased the bubbles gradually changed from a breakup trend to a coalescence trend, and the broken bubbles mostly gathered at the blade pressure surface and impeller outlet.

Throughout the previous exploration of the internal flow of the multiphase pump under gas-liquid two-phase flow conditions, it can be found that scholars at home and abroad have conducted systematic and in-depth research on the multiphase pump based on the fixed size of the bubble, little has been reported on bubble coalescence, breakup and bubble distribution. Due to the relatively complex structure of the impeller passage of the multiphase pump, the dynamics characteristics held by air bubbles at high rotational speeds cannot be ignored.

2 Mathematical model

2.1 Multiphase flow model

On the premise that the calculation accuracy can be guaranteed, the Eulerian-Eulerian two-fluid model is adopted in this paper after considering the phase velocity slip and the phase force. The model can better reflect the phase distribution and the internal flow characteristics of the mixed-transport pump in the gas-liquid two-phase system. The flow process complies with the conservation of mass and momentum, and its governing equations are as follows: Equations 1–4.

$$\frac{Dm}{Dt} = \frac{\partial}{\partial t}(\rho\alpha)_q + \nabla\cdot(\rho\alpha\vec{v})_q = 0 \tag{1}$$

$$\alpha_g + \alpha_l = 1 \tag{2}$$

$$\alpha_g = \frac{Q_g}{Q_g + Q_l} \tag{3}$$

Where, m represents the mass of the phase; ρ represents the density of the phase; $\vec{v}$ is the velocity of the phase; α is the volume fraction of each phase; g is the gas phase, l is the liquid phase; Q is volume flow rate, m^3/s. As shown in Equations 5–9.

$$\frac{D(m\vec{v})_q}{Dt} = \frac{\partial}{\partial t}(\rho\alpha\vec{v})_q + \nabla\cdot(\rho\alpha\vec{v}\vec{v})_q = -\alpha_q\nabla p + \nabla\bar{\bar{\tau}}_q + \alpha_q\rho_q g + \sum_{p=1}^{n}\left(\vec{R}_{pq} + \dot{m}_{pq}\vec{v}_{pq} - \dot{m}_{qp}\vec{v}_{qp}\right) + \vec{M}_{\phi,q} \tag{4}$$

$$\vec{M}_{\phi,q} = \vec{f}_{q,pump} + \left(\vec{f}_{drag,q} + \vec{f}_{vm,q} + \vec{f}_{lift,q}\right) \tag{5}$$

$$\vec{f}_{q,pump} = -\left\{\alpha\rho\left[2\vec{\omega}\times\vec{v}] + \vec{\omega}\times(\vec{\omega}\times\vec{r}) + \frac{D\vec{\omega}}{D_t}\times\vec{r}\right]\right\}_q \tag{6}$$

$$\vec{f}_{drag,q} = \frac{C_D Re}{24} \tag{7}$$

$$C_D = \begin{cases} 24\times\left(1+0.15Re^{0.687}\right)/Re & Re < 1000 \\ 0.44 & Re < 1000 \end{cases} \tag{8}$$

$$Re = \frac{\rho_q\left|\vec{v}_p - \vec{v}_q\right|d_p}{\mu_q} \tag{9}$$

Where, The corner scales q and p stand for phase q and phase p; p is the pressure shared by all phases; $\bar{\bar{\tau}}_q$ is the stress of the phase; $\vec{R}_{pq}$ is an interaction force between phases; $\vec{v}_{pq}$ is the interphase velocity, defined as follows. If $\dot{m}_{pq} > 0$ (that is, phase p mass is being transferred to phase q), $\vec{v}_{pq} = \vec{v}_p$. Likewise, if $\dot{m}_{qp} > 0$ then $\vec{v}_{qp} = \vec{v}_q$, if $\dot{m}_{qp} < 0$ then $\vec{v}_{qp} = \vec{v}_p$; $\vec{f}_{q,pump}$ is the rotational force of the impeller, where $\vec{\omega}$ is the speed of the pump and $\vec{r}$ is the coordinate vector.; $\vec{f}_{drag,q}$ is resistance, the Schiller and Naumann Model was chosen, which is the drag force of the bubble movement in the fluid, also known as drag force, and is related to the size and shape of the bubble and the relative speed between the bubble and the fluid; $\vec{f}_{vm,q}$ is virtual mass force: When bubbles accelerate in the fluid, they drive the fluid to accelerate together. The force to accelerate the bubble not only increases the kinetic energy of the bubble, but also increases the kinetic energy of the fluid. The increase of the kinetic energy of the fluid further promotes the acceleration of the bubble, which is equivalent to the bubble having a virtual additional mass, and the acceleration force is the virtual mass force; The bubble moves in a flow field with velocity difference, and the fluid velocity on different sides of the bubble is different, generating a lift force from low velocity to high velocity on the surface of the bubble, which is represented by $\vec{f}_{lift,q}$.

2.2 Population balance model

The PBM is an effective method for accurately predicting the size and distribution of bubbles in the flow field of a multiphase pump by showing how the size and distribution characteristics of the discrete phases in a gas-liquid two-phase flow system vary from time to time. In a gas-liquid two-phase system, the expressions are: Equation 10.

$$\underbrace{\frac{\partial n(V,t)}{\partial t}}_{\text{time term}} + \underbrace{\nabla\cdot[\vec{u}n(V,t)]}_{\text{convective term}} + \underbrace{\nabla_v\cdot[G_v n(V,t)]}_{\text{effects of mass transfer and pressure changes}} = \underbrace{\frac{1}{2}\int_0^V c(V-V',V')n(V-V',t)n(V',t)dV'}_{\text{birth due to coalescence}} - \underbrace{\int_0^\infty c(V,V')n(V,t)n(V',t)dV'}_{\text{death due to coalescence}} + \underbrace{\int_\nu^\infty b(V')\beta(V|V')n(V',t)dV'}_{\text{birth due to breakup}} - \underbrace{b(V)n(V,t)}_{\text{death due to breakup}} \tag{10}$$

In Equation 7, V' is the volume of the mother bubble; V is the sub-bubble volume; $n(V,t)$ is the bubble number density function with volume V; $c(V,V')$ is the bubble coalescence rate; and $\beta(V|V')$ is the sub-bubble distribution function with volume V. The terms "birth due to coalescence", "death due to coalescence", "birth due to

breakup" and "death due to breakup" represent the birth and death rate of a bubble with a diameter of d.

2.3 Bubble breakup model

In this paper, the bubble breakup behavior was simplified, and it was reasonably assumed that the bubble only broke into two bubbles, and the breakup model of [30] is adopted. In this model, when the energy of the collision between bubbles and turbulent vortices meets a certain relation, bubbles will be broken. The specific expression is as follows: Equations 11–15.

$$P_B(d, f_{BV}, \lambda) = exp\left(-\frac{c_f \pi d^2 \sigma}{\rho_l \frac{4\pi}{3}\left(\frac{\lambda}{2}\right)^3 \frac{\overline{u}_\lambda^2}{2}} \right) \tag{11}$$

$$P_B(d, f_{BV}) = \int_{\lambda min}^{d} P_B(d, f_{BV}, \lambda)\overline{\omega}_{B,\lambda}(d,\lambda)d\lambda, \lambda_{min} = 0.2d \tag{12}$$

$$P_B(d) = \frac{1}{2}\int_0^1 P_B(d, f_{BV}) d f_{BV}, b(V') \tag{13}$$

$$\overline{\omega}_{B,\lambda}(d,\lambda) = \frac{\pi}{4}(d+\lambda)^2 \overline{u_\lambda} \dot{n}_\lambda n_d \tag{14}$$

$$\dot{n}_\lambda = \frac{0.822(1-\alpha)}{\lambda^4} \tag{15}$$

Where, f_{BV} is the volume ratio of one sub-bubble to the parent bubble after the bubble is split into two; $P_B(d, f_{BV}, \lambda)$ is the probability that the energy of the inflow vortex will cause the bubble to break, when the size of the vortex is λ; $P_B(d, f_{BV})$ is the frequency of bubble fracturing when the size range of turbulent vortex is within $[\lambda_{min}, d]$; $b(V')$ 1 and $b(V)$ are the breaking rates of the mother bubble and the sub-bubble, respectively. $P_B(d)$ is the probability of arbitrary bubble break when the size range of turbulent vortex is within $[\lambda_{min}, d]$; $\overline{\omega}_{B,\lambda}(b,\lambda)$ is the average collision frequency between the bubble with diameter d and size λ in unit volume; $\dot{n}_\lambda$ is the number density of turbulent vortices with sizes λ to $\lambda + d\lambda$.

The probability of bubble V' breaking and forming bubbles V is: Equation 16.

$$\beta(V|V') = \frac{P_B(d, f_{BV})}{P_B(d)} \tag{16}$$

The final form of the probability of any bubble V' breaking to generate sub-bubbles V is: Equation 17.

$$\beta(V|V')b(V') = P_B(d, f_{BV})/n_d \tag{17}$$

2.4 Bubble coalescence model

In this paper, the coalescence model of Luo is adopted, and the coalescence probability is the product of the collision frequency and efficiency between bubbles [31]. The specific expression is as follows: Equations 18–23.

$$c(d_i, d_j) = \overline{\omega_c}(d_i, d_j) P_c(d_i, d_j) / \left(n_{d_i}, n_{d_j}\right) \tag{18}$$

$$\overline{\omega_c}(d_i, d_j) = \frac{\pi}{4}\left(d_i + d_j\right)^2 / \overline{u}_{i,j} n_{d_i} n_{d_j} \tag{19}$$

$$\overline{u}_{i,j} = \left(\overline{u}_i^2 + \overline{u}_j^2\right)^{1/2} \tag{20}$$

$$\overline{u}_i = 1.43(\varepsilon d_i)^{1/3} \tag{21}$$

$$P_c(d_i, d_i) = exp\left\{ -c_1 \frac{\left[0.75\left(1 + x_{ij}^2\right)\left(1 + x_{ij}^3\right)\right]^{0.5}}{\left(\frac{\rho_g}{\rho_l} + 0.5\right)^{0.5}\left(1 + x_{ij}^3\right)} We_{ij}^{0.5} \right\} \tag{22}$$

$$We_{ij} = \frac{\rho_l d_i \left(\overline{u}_{ij}\right)^2}{\sigma} \tag{23}$$

Where, c_1 is a constant; $x_{ij} = d_i/d_j$; We_{ij} is Weber number; σ is the surface tension; $\overline{\omega_c}(d_i, d_j)$ is the volume, V_i、 V_j is the frequency of the collision between the two groups of bubbles; $P_c(d_i, d_i)$ is the probability of coalescence of bubbles after collision.

3 Numerical method

3.1 Computing domain model

In this paper, the pressurization unit of the multiphase pump is taken as the research object, and the UG software is used to conduct three-dimensional modeling of the calculation domain [32]. The whole calculation domain consists of four parts: the inlet pipe, the impeller, the diffuser and the outlet pipe. In order to ensure the full development of flow in the inlet and outlet section, the inlet of the impeller and the outlet of the diffuser are extended appropriately, as shown in Figure 1.

3.2 Mesh division

The entire calculation domain is meshed using hexahedral structural meshing techniques. The impeller and guide vane are meshed by TurboGrid software and the inlet and outlet pipes are meshed by ICEM CFD software. Considering the fine structure of the tip clearance and extremely complex flow conditions, the mesh in the radial direction of the tip clearance computational domain is refined. The final mesh division can ensure that the y + value meets the requirements of the turbulence model and accurately analyzes the flow characteristics in the multiphase pump. The specific mesh is shown in Figure 2.

The number of meshes is one of the most important factors affecting the accuracy of numerical simulations, and a reasonable number of meshes is beneficial to the improvement of computational efficiency. In order to eliminate the interference of the number of meshes on the simulation results, this paper took five groups of meshes under the pure water environment to verify the irrelevance, the detailed calculation results are shown in Table 1. In Table 1, H represents the head of the pump, and η represents the efficiency of the pump. It can be seen from Table 1 that the head and efficiency of the multiphase pump gradually become stable with the increase of the number of meshes. When the mesh number is larger than the fourth group, the pump head and efficiency change values are small enough to ignore the influence of the mesh number on the

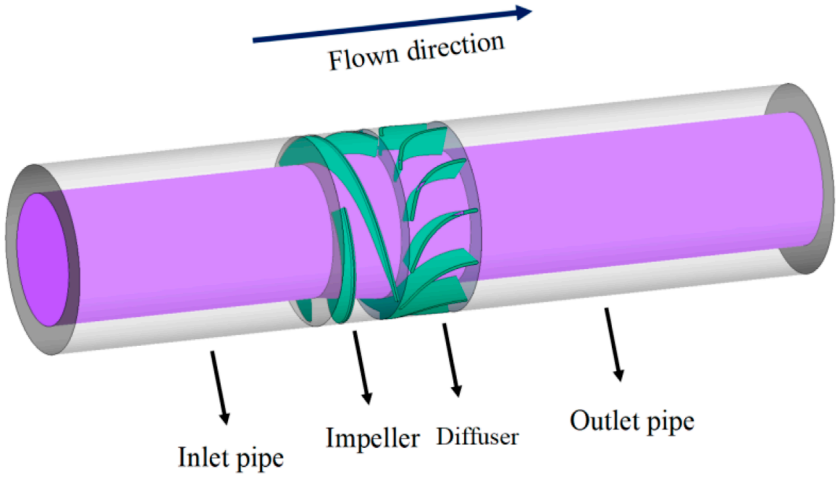

FIGURE 1
Computing domain model.

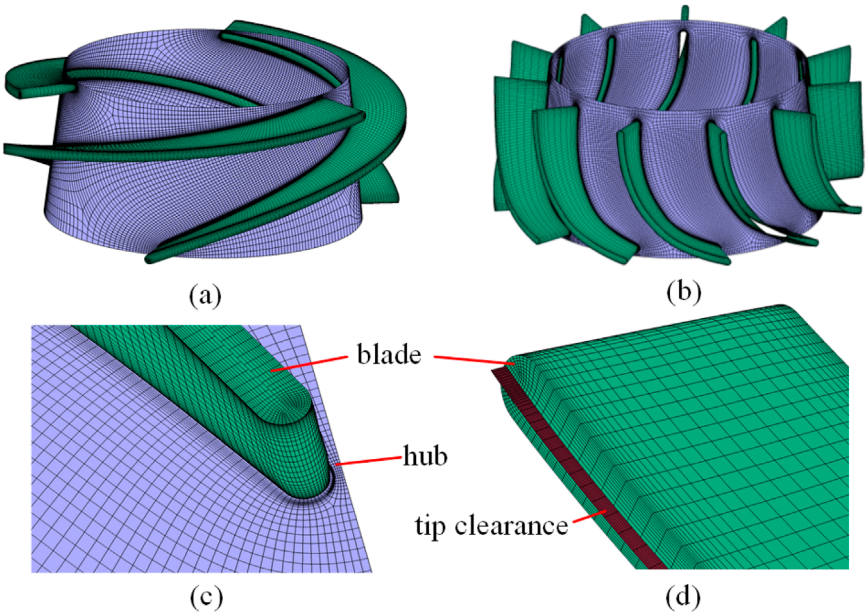

FIGURE 2
Computational domain meshes **(A)** impeller, **(B)** diffuser, **(C)** blade face, **(D)** tip clearance).

calculation. Therefore, considering the calculation resources and calculation accuracy comprehensively, the final mesh number of the calculation domain is 4,606,377.

3.3 CFD-PBM coupling numerical calculation method

In this paper, coupled CFD-PBM calculations are carried out on a hybrid pump with different speed conditions based on FLUENT software, using boundary conditions of velocity inlet and pressure outlet, in order to perform steady, transient and PBM coupled calculations. The Realizable *k-ε* model introduces rotation and curvature related contents into turbulent viscosity, and links turbulent viscosity with strain rate [33]. Compared with the Standard *k-ε* model and the RNG *k-ε* model, it can simulate rotational flow, strong shear flow and separated flow. So the Realizable k-ε model was chosen for numerical simulations in the more complex flow state of the multiphase pump, considering the applicability of the turbulence model and the calculation time. The model is integrated with an angular deformation correction for the vortex viscosity coefficient, which can be better applied to rotating flow fields. Firstly, the Eulerian-Eulerian two-fluid model for two-phase flow is selected for the steady calculation and the kinematic reference system is chosen for the rotating fluid domain. Subsequently, the rotating fluid domain was changed to a dynamic

TABLE 1 Mesh independence verification.

Component	Total mesh	H (m)	η (%)	H/H_1	η/η_1
Mesh1	2,234,518	6.08	35.74	1	1
Mesh2	2,824,192	6.11	35.86	1.0049	1.0034
Mesh3	3,706,406	6.19	36.58	1.0181	1.0240
Mesh4	4,606,377	6.25	37.42	1.0280	1.0470
Mesh5	5,486,700	6.28	37.55	1.0329	1.0506

TABLE 2 Calculate settings.

Item	Number/Content
Solver type	Presure–based
Presure–Velocity Coupling Scheme	SIMPLE
Gradient	Green–Gauss Cell–Based
Pressure	PRESTO!
Density	First Order Upwind
Momentum	First Order Upwind
Turbulent kinetic energy	First Order Upwind
Turbulent dissipation rate	First Order Upwind

grid for the transient calculation, setting the time step to 0.000111 s. The discretization method and relaxation factors in this paper are shown in Table 2. In order to investigate the coalescence and breakup behavior of bubbles in the pressurization unit of the multiphase pump, ten discrete sets of bubble sizes are defined in this paper, with the specific size ranges shown in Table 3.

4 Validation of the numerical simulation method

4.1 Experimental model

In this study, the shape of the pump body was designed as a transparent Plexiglas material with a square exterior and a round interior, and the inlet pipe of the multiphase pump was designed as a transparent pipe to facilitate the observation of the flow effect (as shown in Figure 3). After starting the oil and gas multiphase pump to adjust the gas-liquid flow rate to stabilize the two phases, high-speed photography was used and a special light source was designed to supplement the light (as shown in Figure 4). The main performance indicators of the test instrumentation are shown in Table 4 and the schematic diagram of the multiphase pump test system is detailed in Figure 5.

4.2 Experimental validation

In order to ensure the accuracy of the numerical calculation method and to clearly capture the flow pattern in the pump, this paper has conducted a single-phase and two-phase experimental study of a multiphase pump in turn. Firstly, a transport pump with a tip clearance of 1.0 mm was tested at a speed of 3,000 rpm using pure water as the medium, and the test values of pump head and efficiency were collected on site and combined with the corresponding values obtained from numerical simulations to plot the external characteristics curve of the multiphase pump, as shown in Figure 6. H and η in Figure 6 represent the pump head and efficiency, respectively, and P represents the shaft power of the pump. As can be seen from Figure 6, the error between the test and simulation does not exceed 5% over the range of flow rates tested. This is due to the energy loss during the testing process which inevitably causes the tested values to be smaller than the simulated values, so the numerical calculation method can be considered as an accurate prediction of the energy characteristics of the multiphase pump. Subsequently, the flow pattern of the multiphase pump was tested under gas-liquid two-phase conditions using a mixture of gas and water as the medium.

Figure 7 shows the comparative analysis of the bubble number density (N) of CFD-PBM numerical simulation results and experimental results under different inlet gas volume fractions (IGVF). As illustrated in Figure 7, the simulation results obtained from the coupled CFD-PBM model exhibit a high degree of correlation with the experimental data, with the lift error remaining below 7.5% across all three sets of tested and calculated values. The position of high bubble number in the flow channel of the mixed transport pump in Figure 7 is basically consistent with the photos taken in the test. It can be seen that the numerical calculation method used in this paper is highly reliable. In subsequent studies, the research was conducted at a gas fraction of 9% for the inlet gas.

5 Analysis of results

5.1 Effect of speed on bubble distribution

In order to investigate the formation mechanism of the gas-liquid distribution, it is important to understand the distribution characteristics of the bubbles in the multiphase pump. The medium

TABLE 3 Discrete bubble sizes.

Bin	Bin- 0	Bin-1	Bin-2	Bin-3	Bin-4	Bin-5	Bin-6	Bin-7	Bin-8	Bin-9
Diameter/mm	10	5.9949	3.5938	2.1544	1.2916	0.774	0.464	0.278	0.167	0.1

FIGURE 3
Test system.

FIGURE 4
High-speed photography.

size Bin4 (1.2916 mm) in the discrete bubble has been set as the inlet bubble in the calculations before the flow characteristics of the multiphase pump are analyzed, and the bubble size distribution in the multiphase pump can be easily obtained based on the coupled CFD-PBM model. For the purpose of the following analysis, the following ten groups of bubbles are divided into three categories of bubbles: large, medium and small. Four groups of bubbles from Bin0 to Bin3 are large bubbles, three groups of bubbles from Bin4 to Bin6 are medium bubbles and three groups of bubbles from Bin7 to Bin9 are small bubbles. Figure 8 shows the bubble distribution within

TABLE 4 Main parameters of multiphase pump.

Parameters	Symbol	Value	Unit
Design flow rate	Q_d	90	m^3/h
Design speed	n	3,000	rpm
Number of impeller blades	Z_1	3	(–)
Number of diffuser blades	Z_2	11	(–)
Hub/shroud ratio	$\bar{d}$	0.7	(–)
Inner diameter	D	161	mm
Head	H	10.5	m

the pressurization unit of the multiphase pump for different speed conditions. As can be seen in Figure 8, the bubble distribution in the impeller and blade domains show a similar trend throughout the pressurization unit. The volume fraction of large bubbles larger than Bin4 in the pressurization unit of the mixing pump decreases with increasing speed, while the volume fraction of small and medium bubbles in the group smaller than Bin4 is positively correlated with speed. It can also be found that the distribution pattern of the volume fraction of large bubbles is highly consistent throughout the pressurization unit. In the blade domain, however, the large number of vortices formed due to the special structure makes the tendency of bubble breakup significantly stronger, and the bubble percentage in the Bin5 to Bin7 groups is significantly more than in the impeller domain, but the bubble content in the Bin8 to Bin9 groups is significantly lower than in the impeller domain. This further demonstrates the inconsistent tendency for bubbles to be broken by different external influences, with the shearing effect of the blades in the pressurization unit being significantly stronger than the effect of the vortices generated in the diffuser on bubble breakup.

5.2 Effect of speed on the coalescence and breakup behavior of bubbles

To further reveal the effect of speed on the coalescence and breakup behavior of bubbles in the flow passage, this paper uses an equivalent surface in which the average bubble size is greater than or equal to the size of the impeller inlet bubble to represent the coalescence zone of bubbles in the flow passage, and *vice versa* to represent the bubble breakup zone. Figure 9 shows the distribution of bubble coalescence and breakup at the 0.5 blade height in the pressurization unit of the multiphase pump. Among

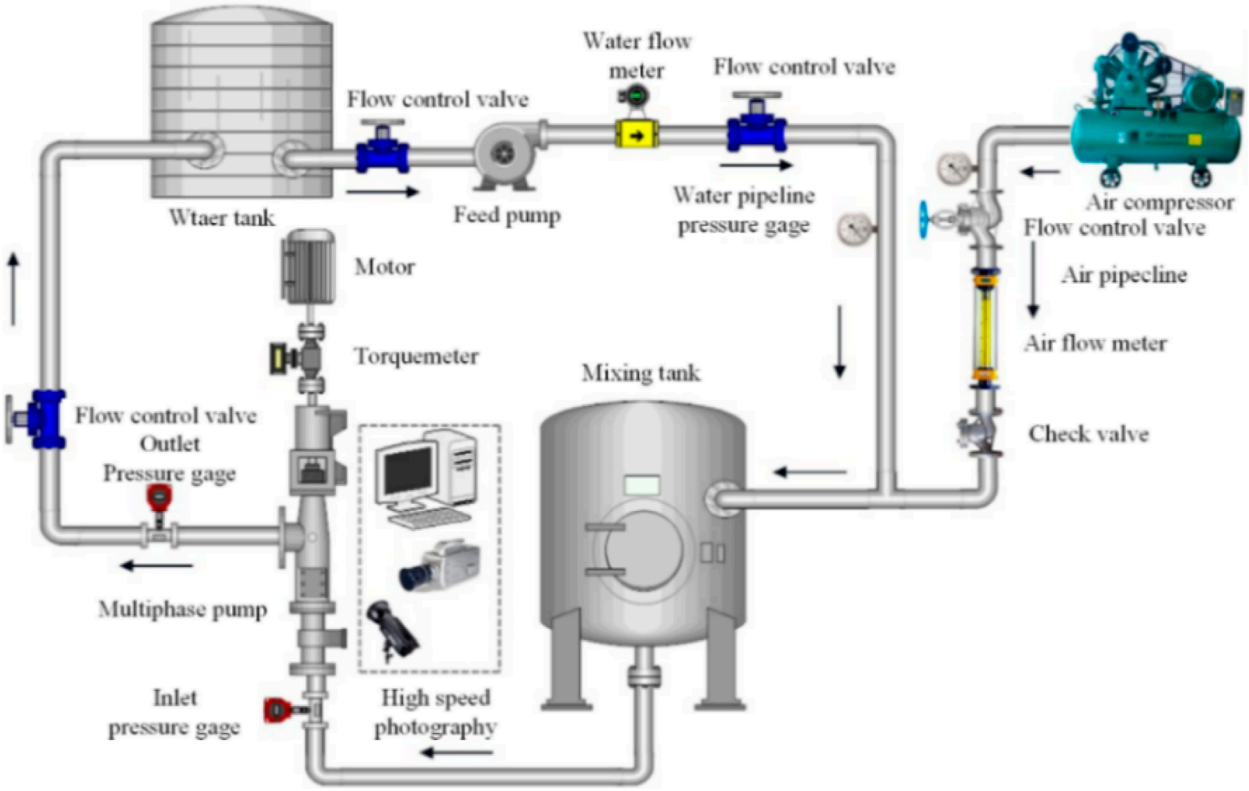

FIGURE 5
Schematic diagram of the test system.

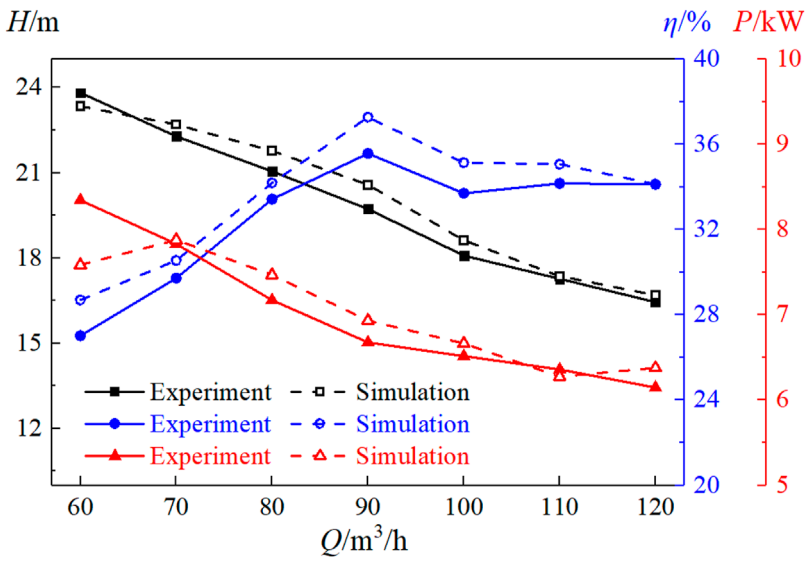

FIGURE 6
Comparison of external characteristics of the experiment and numerical simulation.

them, the larger the average bubble size in the coalescence zone and the smaller the size in the breakup zone, the greater the degree of coalescence and breakup. From Figure 9, it is easy to find that the large bubbles in the coalescence zone are mainly located on the suction side of the impeller blade and the pressure side of the diffuser blade, and the small bubbles in the crushing area mainly cover the pressure side of the impeller blade and the suction side of the guide blade. This may be due to the fact that

10.3389/fphy.2024.1498648

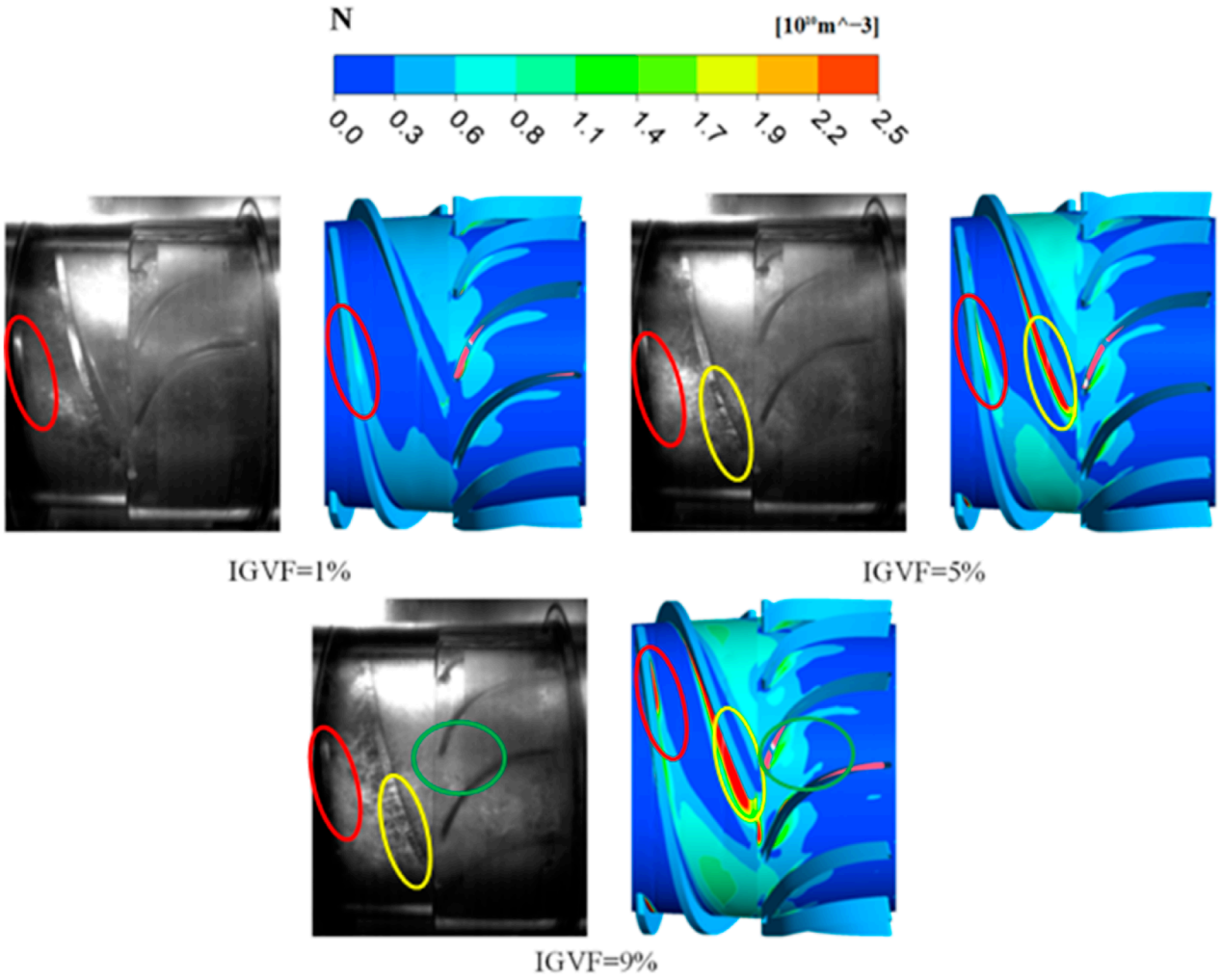

FIGURE 7
Numerical simulation results of CFD-PBM under different inlet gas volume fractions compared with the experimental bubble number density analysis.

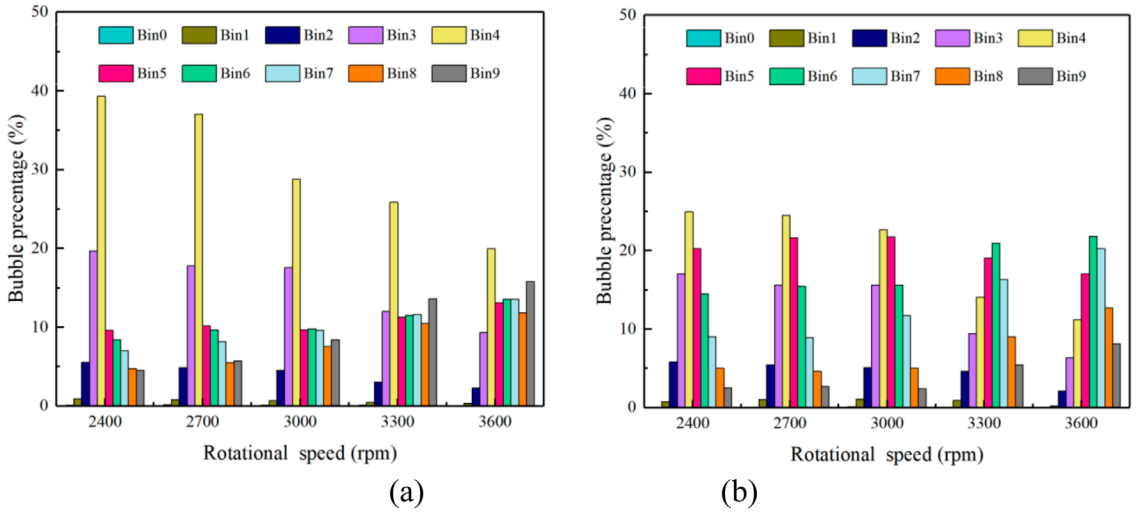

FIGURE 8
Distribution of bubbles in the pressurization unit of the multiphase pump at different speed conditions. **(A)**Impeller, **(B)**Diffuser.

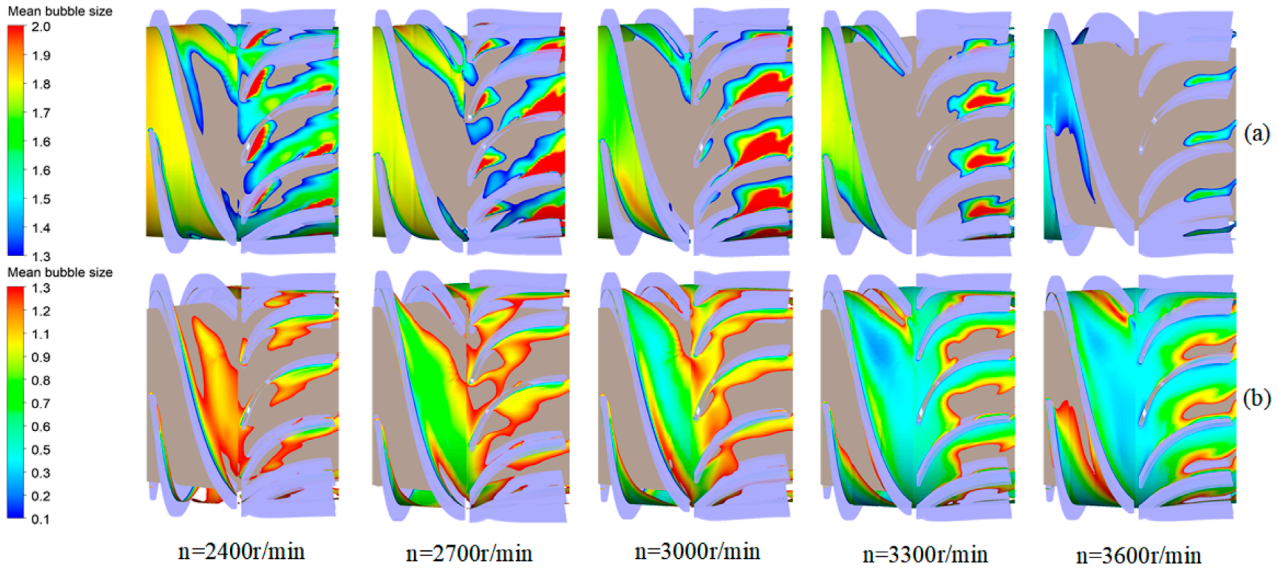

FIGURE 9
Distribution of bubble coalescence and breakup zones in the pressurization unit of the multiphase pump at different speeds. **(A)** Bubble coalescence zone, **(B)** bubble breakup zone.

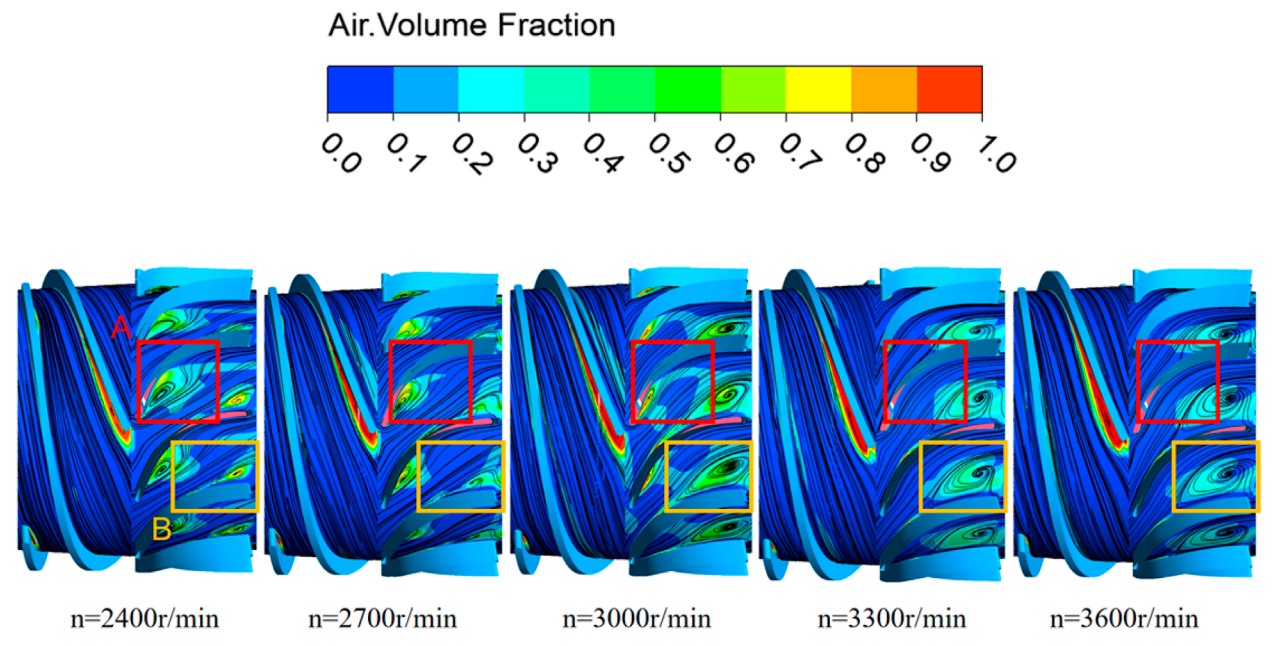

FIGURE 10
Gas phase and streamline distribution in the pressurization unit of the multiphase pump under different speed conditions.

the large bubbles have a larger gas phase content and are mainly adsorbed on the low pressure side of the blade by the pressure gradient within the impeller, while the small bubbles are subjected to a combination of forces within the pressurization unit that cause their trajectory and distribution characteristics to change. In addition, as can be seen in Figure 9A, the increase in speed significantly inhibits the coalescence behavior of the bubbles and the domain of coalescence is significantly reduced. Specifically, the bubble coalescence zone in the impeller domain decreases along the axial direction parallel to the blade profile with the increase of rotational speed, and the degree of bubble coalescence weakens accordingly. The bubble coalescence zone in the diffuser domain

FIGURE 11
Schematic diagram of pressurization unit division of multiphase pump.

is reduced along the axial direction, and the bubble coalescence degree reaches the strongest in the design condition, and the bubble coalescence behavior almost does not occur in the high speed condition. As can be seen from Figure 9B, the bubble breakup zone is just complementary to the coalescence zone, and the law is opposite. Under low speed conditions, fewer bubbles undergo breakup behavior, less shearing by the blades and only sporadic crushing behavior occurs near the blade surface. As the speed increases, the shearing effect intensifies sharply, the turbulence in the flow field increases in intensity, the shear stress on the bubbles increases and most of the area within the domain of the pressurization unit is filled with broken bubbles.

5.3 Effect of speed on gas phase distribution and vortex structure

Figure 10 shows the distribution of the gas phase and flow lines in the pressurization unit of the multiphase pump under different speed conditions, for the purpose of later discussion the vortices at the leading and trailing edges of the diffuser are noted as vortex A and B, and have been marked with red and orange wireframes respectively. As can be seen in Figure 10, the distribution of the gas phase in the impeller domain passage is generally similar at all operating conditions and the flow patterns are good. The gas phases are all gathered on the suction side of the blade by the pressure gradient and some of the small vortices, and the increase in speed results in a more gentle increase in the degree of gather. In contrast, the gas phase distribution and flow state in the diffuser show obvious change rules under the change of speed. It is not difficult to find that vortex A gradually weakens with the increase of speed, the gas phase it enrolls decreases correspondingly, and vortex B and vortex A show exactly opposite change rules. This is because under the condition of low speed, the fluid at the outlet of the impeller diverts towards the pressure surface and suction surface of the diffuser, and the diverting liquid mixes with each other to form vortex A. Because of its special structure, the guide vane forms a vortex B at the tail of the guide vane to provide a velocity circulation. And the increase in speed makes the impeller outlet liquid flow angle change, impeller outlet at the diffuser pressure surface diversion phenomenon weakened, vortex A gradually disappeared, vortex B gradually enhanced. That is to say, the vortex A, B is a pair of mutually separate vortex, inevitably show the opposite law of change.

5.4 Influence of speed on gas-liquid velocity difference and pressure distribution

In order to further explore the internal flow law of the multiphase pump, the impeller and diffuser in the pressurization unit are evenly divided into 11 planes along the axial direction from the inlet, among which plane 1 is the inlet surface and plane 11 is the outlet surface, as shown in Figure 11.

In order to quantitatively analysis the distribution of flow characteristics in the axial direction in the pressurization unit of the multiphase pump, the characteristic parameters in the different planes classified above are analyzed. Figure 12 shows the difference in gas-liquid velocity slip (gas phase velocity minus liquid phase velocity) and the pressure distribution along the axial direction in the booster unit of the multiphase pump at different speed at the inlet gas volume fraction of 9%. As can be seen in Figure 12, the effect of speed on the gas-liquid velocity difference within the pressurization unit of the multiphase pump is not consistent in the impeller and diffuser domains. The gas phase velocity is significantly greater than the liquid phase velocity at the impeller inlet and dynamic-static interface, while the gas phase velocity is less than the liquid phase velocity at the remaining axial positions. The increase in impeller speed results in the generation of more small bubbles in the impeller domain to promote the homogeneity of the gas-liquid mixing, the amplitude of the gas-liquid velocity difference curve is significantly reduced and the velocity slip phenomenon is correspondingly weakened. The velocity difference between gas and liquid in the diffuser is mainly influenced by the vortex in the flow passage. The increase in speed accelerates the formation of vortex inside the diffuser, and the vortex center attracts a large number of bubbles to intensify the phenomenon that makes the two phases of gas and liquid separate. It can also be seen in Figure 12 that the speed has a significantly greater effect on the pressure distribution in the impeller, the core work component of the multiphase pump, than in the diffuser domain, and that an increase in speed significantly increases the pressure pressurization performance of the multiphase pump. The diffuser, as a rectification component, is minimally affected by the speed of rotation, except for the obvious pressure fluctuations that occur at the dynamic-static interface.

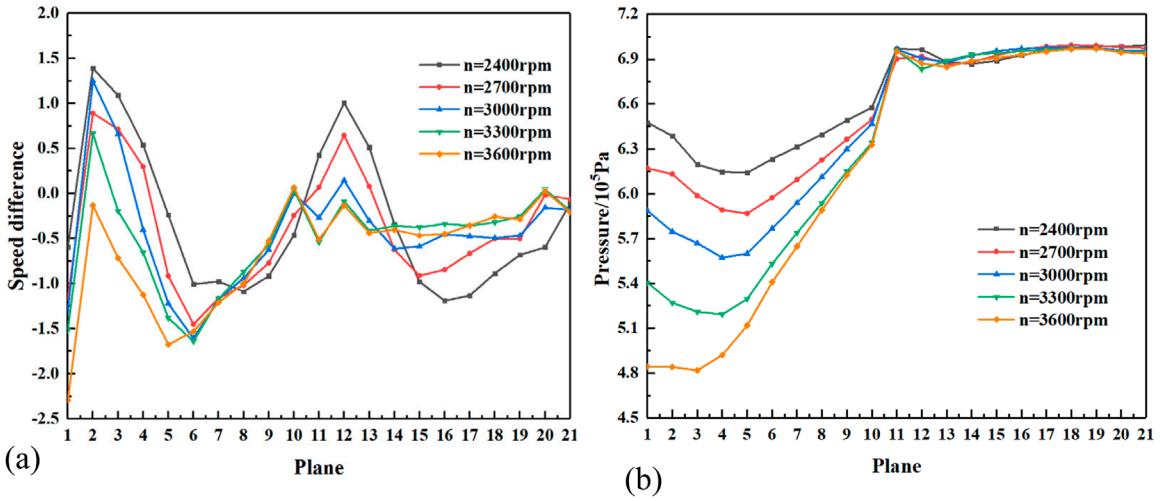

FIGURE 12
Axial gas-liquid velocity slip difference and pressure distribution in the pressurization unit of the multiphase pump at different speeds. **(A)** Gas-liquid velocity difference, **(B)** pressure distribution.

6 Conclusion

In order to grasp the internal flow law and prediction performance of the multiphase pump more accurately, the parameters of the flow field in the pump were solved based on the CFD-PBM coupling model. By analyzing the laws of bubble distribution, gas phase distribution, vortex structure and gas-liquid velocity difference in the pressurization unit of the multiphase pump, the influence of speed on the internal flow characteristics of the multiphase pump was revealed. The main conclusions are as follows:

(1) The volume fraction of large air bubbles in the pressurization unit of the multiphase pump decreases significantly with speed, while the opposite is true for small bubbles. At high speed, bubbles are more likely to break due to blade shear, and the effect of shear on bubble breaking behavior is obviously stronger than that of vortex entrainment.

(2) The bubble coalescence zone in the pressurization unit of the multiphase pump covers the impeller suction surface and diffuser pressure surface, and the law of the breakup zone is opposite to the coalescing zone. Bubble coalescing occurs in a large area of the pump under low speed conditions, and only a few crushing behaviors occur near the surface of the blade. With the increase of rotational speed, the bubble coalescence zone will shrink along the axial direction parallel to the blade profile, and the bubble breakup zone will almost cover the whole domain.

(3) The influence of speed in the pressurization unit of the multiphase pump on the gas phase distribution and vortex structure in the diffuser domain is significantly greater than that in the impeller domain, and the impeller domain has fewer vortices and less gas phase gather. Under the influence of the speed of the flow passage in the diffuser domain, A and B mutually separate vortices are formed at the leading edge and trailing edge of the diffuser. The gas phase is attracted by the vortex and gathers near the vortex center in a large range, and the speed promotes the formation of vortex B.

(4) The increase of speed in the impeller domain promotes the uniformity of gas-liquid mixing and weakens the velocity slip. Under the influence of the structure of diffuser, the speed accelerates the formation of the vortex, which intensifies the velocity slip. The influence of speed on the pressure distribution is mainly reflected in the impeller domain. The increase of speed obviously increases the pressurization performance of the multiphase pump.

Data availability statement

The original contributions presented in the study are included in the article/supplementary material, further inquiries can be directed to the corresponding authors.

Author contributions

XG: Conceptualization, Methodology, Software, Validation, Visualization, Writing–original draft, Writing–review and editing. SHI Guangtai: Conceptualization, Data curation, Formal Analysis, Funding acquisition, Investigation, Project administration, Visualization, Writing–review and editing. HC: Conceptualization, Resources, Supervision, Validation, Writing–review and editing.

WL: Formal Analysis, Methodology, Resources, Software, Writing–review and editing. JF: Data curation, Funding acquisition, Investigation, Software, Supervision, Validation, Writing–review and editing.

Funding

The author(s) declare that financial support was received for the research, authorship, and/or publication of this article. This work was supported by the Sichuan Natural Science Foundation Outstanding Youth Science Foundation (2024NSFJQ0012), the Key project of Regional Innovation and Development Joint Fund of National Natural Science Foundation (U23A20669) and the Sichuan Science and Technology Program (2022ZDZX0041).

Conflict of interest

The authors declare that the research was conducted in the absence of any commercial or financial relationships that could be construed as a potential conflict of interest.

Publisher's note

References

1. Serena A, Bakken LE. Design of a multiphase pump test laboratory allowing to perform flow visualization and instability analysis. In: *POWER 2015 (ASME 2015 power conference)* (2015). doi:10.1115/POWER2015-49769

2. Lea JF, Bearden JL. Effect of gaseous fluids on submersible pump performance. *J Pet Tech* (1982) 34:2922–30. doi:10.2118/9218-PA

3. Schäfer T, Bieberle A, Neumann M, Hampel U. Application of gamma-ray computed tomography for the analysis of gas holdup distributions in centrifugal pumps. *Flow Meas Instrumentation* (2015) 46:262–7. doi:10.1016/j.flowmeasinst.2015.06.001

4. Tao S, Shi G, Xiao Y, Huang Z, Wen H. Effect of operating parameters on the coalescence and breakup of bubbles in a multiphase pump based on a CFD-PBM coupled model. *J Mar Sci Eng* (2022) 10:1693. doi:10.3390/jmse10111693

5. Murakami M, Minemura K. Effects of entrained air on the performance of a centrifugal pump: 1st report, performance and flow conditions. *Bull JSME* (1974) 17:1047–55. doi:10.1299/jsme1958.17.1047

6. Murakami M, Minemura K. Effects of entrained air on the performance of centrifugal pumps: 2nd report, effects of number of blades. *Bull JSME* (1974) 17:1286–95. doi:10.1299/jsme1958.17.1286

7. Sekoguchi K, Takada S, Kanemori Y. Study of air-water two-phase centrifugal pump by means of electric resistivity probe technique for void fraction measurement: 1st report, measurement of void fraction distribution in a radial flow impeller. *Bull JSME* (1984) 27:931–8. doi:10.1299/jsme1958.27.931

8. Shao C, Li C, Zhou J. Experimental investigation of flow patterns and external performance of a centrifugal pump that transports gas-liquid two-phase mixtures. *Int J Heat Fluid Flow* (2018) 71:460–9. doi:10.1016/j.ijheatfluidflow.2018.05.011

9. Zhang J, Cai S, Li Y, Zhu H, Zhang Y. Visualization study of gas–liquid two-phase flow patterns inside a three-stage rotodynamic multiphase pump. *Exp Therm Fluid Sci* (2016) 70:125–38. doi:10.1016/j.expthermflusci.2015.08.013

10. Stel H, Ofuchi EM, Sabino RHG, Ancajima FC, Bertoldi D, Marcelino Neto MA, et al. Investigation of the motion of bubbles in a centrifugal pump impeller. *J Fluids Eng* (2018) 141. doi:10.1115/1.4041230

11. Shah SR, Jain SV, Patel RN, Lakhera VJ. CFD for centrifugal pumps: a review of the state-of-the-art. *Proced Eng* (2013) 51:715–20. doi:10.1016/j.proeng.2013.01.102

12. Li W, Long Y, Ji L, Li H, Li S, Chen Y, et al. Effect of circumferential spokes on the rotating stall flow field of mixed-flow pump. *Energy* (2024) 290:130260. doi:10.1016/j.energy.2024.130260

13. Li W, Yang Q, Yang Y, Ji L, Shi W, Agarwal R. Optimization of pump transient energy characteristics based on response surface optimization model and computational fluid dynamics. *Appl Energ* (2024) 362:123038. doi:10.1016/j.apenergy.2024.123038

14. Minemura K, Uchiyama T. Three-dimensional calculation of air-water two-phase flow in centrifugal pump impeller based on a bubbly flow model. *J Fluids Eng* (1993) 115:766–71. doi:10.1115/1.2910210

15. Kiyoshi M, Uchiyama T. Three dimension calculation of air water two-phase flow in centrifugal pump impeller based on a bubbly flow model with fixed cavity. *JSME Intenral J Ser B* (1994) 37:726–35.

16. Caridad J, Kenyery F. CFD analysis of electric submersible pumps (ESP) handling two-phase mixtures. *J Energ Resour Tech* (2004) 126:99–104. doi:10.1115/1.1725156

17. Caridad J, Asuaje M, Kenyery F, Tremante A, Aguillón O. Characterization of a centrifugal pump impeller under two-phase flow conditions. *J Pet Sci Eng* (2008) 63:18–22. doi:10.1016/j.petrol.2008.06.005

18. Müller T, Limbach P, Skoda R. Numerical 3D RANS simulation of gas-liquid flow in a centrifugal pump with an Euler-Euler two-phase model and a dispersed phase distribution. In: *11 th European conference on turbomachinery fluid dynamics and thermodynamics European turbomachinery society* (2015).

19. Tremante A, Moreno N, Rey R, Noguera R. Numerical turbulent simulation of the two-phase flow (liquid/gas) through a cascade of an axial pump. *J Fluids Eng* (2002) 124:371–6. doi:10.1115/1.1471533

20. Zhu J, Guo X, Liang F, Zhang H-Q. Experimental study and mechanistic modeling of pressure surging in electrical submersible pump. *J Nat Gas Sci Eng* (2017) 45:625–36. doi:10.1016/j.jngse.2017.06.027

21. Barrios L, Prado MG, Kenyery F. CFD modeling inside an electrical submersible pump in two-phase flow condition. *FEDSM* (2009) 1:457–69. doi:10.1115/FEDSM2009-78492

22. Barrios L. *Visualization and modeling of multiphase performance inside an electrical submersible pump*. ProQuest: The University of Tulsa (2007).

23. Barrios L, Prado MG. Experimental visualization of two-phase flow inside an electrical submersible pump stage. *J Energ Resour Tech* (2011) 133. doi:10.1115/1.4004966

24. Hulburt HM, Katz S. Some problems in particle technology: a statistical mechanical formulation. *Chem Eng Sci* (1964) 19:555–74. doi:10.1016/0009-2509(64)85047-8

25. Wang T, Wang J, Jin Y. Experimental study and CFD simulation of hydrodynamic behaviours in an external loop airlift slurry reactor. *Can J Chem Eng* (2004) 82:1183–90. doi:10.1002/cjce.5450820605

26. Wang T, Wang J, Jin Y. A CFD–PBM coupled model for gas–liquid flows. *AIChE J* (2006) 52:125–40. doi:10.1002/aic.10611

27. Xing C. *Experimental study of bubble bed reactor and numerical simulation of CFD-PBM coupling model*. Beijing China: Tsinghua University (2014).

28. Chen Y, Patil A, Chen Y, Bai C, Wang Y, Morrison G. Numerical study on the first stage head degradation in an electrical submersible pump with population balance model. *J Energ Resour Tech* (2018) 141. doi:10.1115/1.4041408

29. Yan S, Sun S, Luo X, Chen S, Li C, Feng J. Numerical investigation on bubble distribution of a multistage centrifugal pump based on a population balance model. *Energies* (2020) 13:908. doi:10.3390/en13040908

30. Luo H. *Coalescence, breakup and liquid circulation in bubble column reactors*. Trondheim: The University of Trondheim (1995).

31. Luo H, Svendsen HF. Theoretical model for drop and bubble breakup in turbulent dispersions. *AIChE J* (1996) 42:1225–33. doi:10.1002/aic.690420505

32. Shu Z, Shi G, Tao S, Tang W, Li C. Three-dimensional spatial-temporal evolution and dynamics of the tip leakage vortex in an oil–gas multiphase pump. *Phys Fluids* (2021) 33:113320. doi:10.1063/5.0073634

33. Shih T-H, Liou WW, Shabbir A, Yang Z, Zhu J. A new k-ϵ eddy viscosity model for high Reynolds number turbulent flows. *Comput and Fluids* (1995) 24:227–38. doi:10.1016/0045-7930(94)00032-T